Vertically Integrated Coaxial Resonator-Based Multiband Bandpass Filters Using SLA 3-D Printing

Kunchen Zhao, *Graduate Student Member, IEEE*, and Dimitra Psychogiou, *Senior Member, IEEE*

***Abstract*— This letter reports on a novel multiband RF filtering concept and a compact low-loss integration scheme for coaxial resonator-based multiband bandpass filters (BPFs). Size compactness is achieved by: 1) vertically stacking its constituent resonators, so that the available 3-D volume is optimally occupied; 2) the use of subwavelength capacitively loaded coaxial resonators; and 3) monolithic integration enabled by stereolithography apparatus (SLA) additive manufacturing (AM). A unique coupling routing diagram (CRD) is proposed and implemented with capacitively loaded coaxial resonators that allow to independently control the passband and stopband frequencies and facilitate both symmetric and asymmetric responses. A dual-band and triple-band BPFs operating at sub-6 GHz were designed, manufactured, and tested demonstrating highly miniaturized form factors and passbands with in-band insertion loss (IL) < 0.2–0.3 dB, i.e., Q_{eff}: 640–1030.**

***Index Terms*— 3-D printing, bandpass filters (BPFs), coaxial resonators, high-Q resonators, multiband filters.**

I. Introduction

THE unprecedented growth of wireless communications is calling for RF systems able to support multiple applications and high data rates. In these systems, bandpass filters (BPFs) with high quality factor (Q), high selectivity, and multiband functionality are in need. For space- or terrestrial-based stations, lightweight and size compactness are other important metrics. The majority of multiband BPFs to date have been implemented using planar microstrip [1] or substrate-integrated waveguide architectures [2] that exhibit high insertion loss (IL) (2–4 dB) and limited power handling capabilities. Waveguide-based fully metallic filters [3] have lower IL and can handle higher power. However, they are based on multipart integration solutions that are bulky and expensive.

Coaxial cavity resonator-based filters are preferred for satellite or base-station applications due to their small size, low-loss, and wide spurious-free range [4]. Most of the existing coaxial multiband BPFs are based on multimode or stepped-impedance resonators [5], [6], [7], [8] that are hard to be extended to more than two bands. Multiband configurations where a narrow set of frequencies are notched out from a wide passband have been shown in [9] and [10]. Although they exhibit a greater number of passbands (>2), they require large number of resonators that result in increased volume and high manufacturing cost.

Manuscript received 9 February 2023; revised 10 March 2023; accepted 11 March 2023. Date of publication 27 March 2023; date of current version 7 July 2023. This work was supported by the Ireland Science Foundation (SFI) under Grant 20/RP/8334. *(Corresponding author: Dimitra Psychogiou.)*

Kunchen Zhao is with the Department of Electrical, Computer and Energy Engineering, University of Colorado, Boulder, CO 80309 USA (e-mail: kunchen.zhao@colorado.edu).

Dimitra Psychogiou is with the School of Engineering, University College Cork, Cork, T12 K8AF Ireland, and also with the Tyndall National Institute, Cork, T12 R5CP Ireland (e-mail: dpsychogiou@ucc.ie).

Color versions of one or more figures in this letter are available at https://doi.org/10.1109/LMWT.2023.3257765.

Digital Object Identifier 10.1109/LMWT.2023.3257765

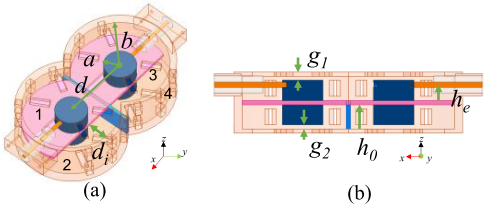

Fig. 1. EM simulation model of the dual-band BPF with vertically integrated capacitively loaded coaxial resonators. (a) Bird-eye view. (b) Side view. Dimensions $a = 5$, $b = 15$, $h_0 = 6$, $h_e = 3.9$, $g_1 = 1$, $g_2 = 1$, $d = 20$, and $d_i = 10$ (unit: millimeters).

Additive manufacturing (AM) techniques are increasingly used for RF filters due to their low cost, fast turnaround time, and ability to manufacture complex geometries. Among them, stereolithography apparatus (SLA) has gained popularity due being easily accessible and leading to parts with low surface roughness, yet it has mostly been used as a replacement of conventional multipart computer numerical control (CNC) machining. Although it is fairly straightforward to manufacture monolithic waveguides [11], [12], most of the 3-D coaxial filters have been materialized as split blocks due to their geometrical complexity [13], [14]. A monolithic integration approach using SLA was demonstrated in [10] for in-line multiband BPFs. In [15], vertically integrated coaxial BPFs were presented with significantly reduced size; however, they were only shown for single-band topologies.

Expanding upon [10] and [15], this letter explores the potential to realize highly miniaturized vertically integrated multiband filters using coaxial-resonator-based configurations alongside a novel compact monolithic integration scheme for single SLA printing. The proposed multiband concept exhibits the following unique characteristics: 1) compact size and minimized (8× improvement) axial ratio (AR) enabled by vertical integration of subwavelength coaxial resonators; 2) combined use of inline and vertical couplings within the 3-D volume of the filter; 3) transfer functions with independently controlled passbands and stopbands; and 4) monolithic integration facilitated by SLA manufacturing.

II. Theoretical Foundations

A. Dual-Band Filter Concept and Vertical Integration Scheme

A conceptual illustration and the 3-D electromagnetic (EM) model of the proposed vertically integrated dual-band second-order BPF is shown in Fig. 1. It is based on four capacitively

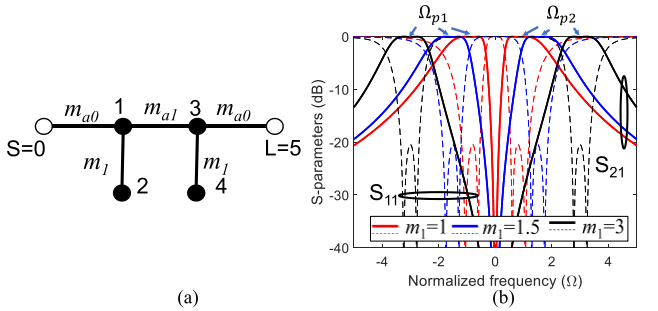

Fig. 2. Second-order dual-band BPF. (a) CRD. (b) Synthesized response for different values of m_1 showing reconfigurability of the passband frequency. In all examples, $m_{a0} = 1.1$ and $m_{a1} = 1$.

loaded coaxial resonators, namely, two in-line resonators (res. 1 and 3) and two shunt resonators (res. 2 and 4) that are vertically stacked with the in-line ones. The dual-band BPF has two second-order bands and functionalizes the coupling routing diagram (CRD) in Fig. 2. For each resonator, the center frequency is determined by the size of the capacitive gap g and the radius ratio of the cavity wall b and the center post a. The RF signal is inserted in the cavity by tapping the SMA connector to the post of the first resonator. This also acts as the external coupling (m_{a0} in Fig. 2), whose magnitude is controlled by the height of the SMA h_e. The interresonator coupling between the in-line resonators 1 and 3 (m_{a1} in Fig. 2) is provided by the coupling iris [10]. For each pair of vertically stacked resonators (e.g., 1 and 2), the interresonator coupling m_1 is materialized by partially removing their shared ground plane and its magnitude is controlled by the size of the coupling window d_i [15]. A septum is added between resonators 2 and 4 to prevent coupling between them.

The theoretical synthesized response is depicted in Fig. 2(b) for different m_1 values. To obtain a dual-band transfer function, all resonators need to be synchronously tuned at $\Omega = 0$, and the center frequency of the two passband is determined using the following equation:

$$\Omega_{p1,2} = \pm|m_1|. \tag{1}$$

Using as a basis this CRD, a dual-band BPF was designed for $m_{a0} = 1.1$, $m_{a1} = 1$, and $m_1 = 1$ and two bands centered at $f_{c1} = 3.70$ and $f_{c2} = 4.15$ GHz with fractional bandwidths (FBWs) $\text{FBW}_1 = 10.3\%$ and $\text{FBW}_1 = 8.0\%$, respectively. The performance of the filter is analyzed by EM simulations in ANSYS HFSS. Its dimensions are listed in Fig. 1. To characterize the effective usage of volume of a 3-D object, the metric of AR in the following equation is used:

$$\text{AR} = \frac{\text{Max size in } x-y \text{ plane}}{\text{Height in } z \text{ axis}}. \tag{2}$$

Note that for a given cubic space, the optimal AR is $(2)^{1/2}$. Based on this definition, the AR of the vertically integrated dual-band BPF has been calculated equal to 3.5. If compared with a conventional dual-band BPF integration of the CRD in Fig. 2, where all resonators placed on the same horizontal plane, the AR would be 10.9. Therefore, a 3× AR improvement can be obtained by using the proposed vertical integration concept.

B. Triple-Band Filter Concept

To explore the scalability of the vertically stacked multiband concept, a second-order triple-band prototype was designed in

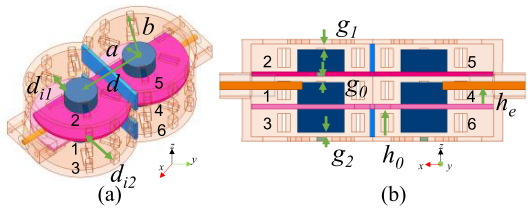

Fig. 3. 3-D model of the triple-band BPF. (a) Bird-eye view. (b) Side view. $a = 5$, $b = 15$, $h_0 = 6$, $h_e = 4$, $g_1 = 1.2$, $g_2 = 0.9$, $g_0 = 1.25$, $d = 22.2$, $d_{i1} = 10$, and $d_{i2} = 10$ (unit: millimeters).

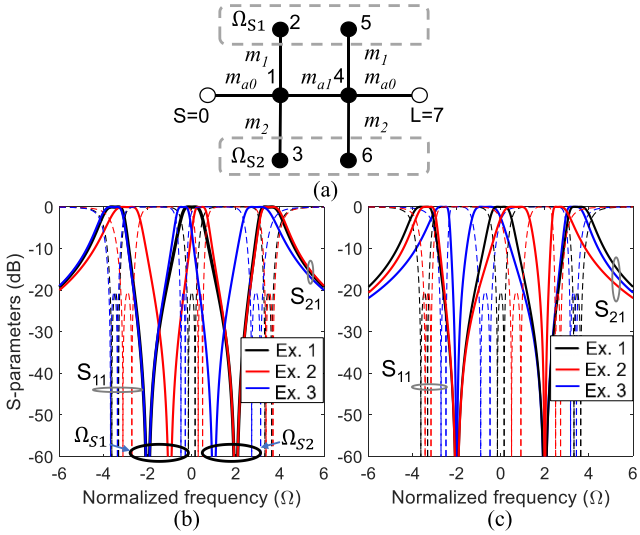

Fig. 4. Second-order triple-band BPF. (a) CRD. (b) Synthesized response for different resonant frequencies of the shunt resonators showing stopband tuning. Ex. 1: $m_{2,2} = m_{5,5} = -m_{3,3} = -m_{6,6} = 2$. Ex. 2: $m_{2,2} = m_{5,5} = 1$ and $m_{3,3} = m_{6,6} = -2$. Ex. 3: $m_{2,2} = m_{5,5} = 2$ and $m_{3,3} = m_{6,6} = -1$. (c) Synthesized response for different values of m_1 showing passband tuning. Ex. 1: $m_1 = m_2 = 2$. Ex. 2: $m_1 = 2$ and $m_2 = 1$. Ex. 3: $m_1 = 1$ and $m_2 = 2$. In all examples, $m_{a0} = 1.1$, $m_{a1} = 1$, and $m_{1,1} = m_{4,4} = 0$.

Fig. 3 based on the CRD in Fig. 4. A similar CRD has been shown in [16], however, for multibandstop microstrip filters. Compared to the dual-band case, an additional shunt resonator is added at the other side of each in-line resonator to create an additional stopband. The frequencies of the stopbands $\Omega_{S1,2}$ are determined by the resonance of the shunt resonators using the following equation:

$$\Omega_{S1} = -m_{2,2} = -m_{5,5} \quad \text{and} \quad \Omega_{S2} = -m_{3,3} = -m_{6,6}. \tag{3}$$

As shown in Fig. 4(b), the stopbands can be tuned independently and by only altering the resonant frequencies of their shunt resonators (i.e., 2 and 5 for Ω_{S1} and 3 and 6 for Ω_{S2}). The bandwidth (BW) of each passband may be altered when tuning the shunt resonators. However, the BW change can be counteracted by tuning the frequency of the in-line resonators or m_1 and m_2, as shown in the synthesized example cases in Fig. 4.

Fig. 4(c) exhibits the transfer function dependence on m_1 and m_2. By altering m_1 and m_2, the separation between the passbands can be controlled, where increasing their magnitude leads to lager separation. Compared to a multiband CRD topology where all shunt resonators are placed on the same side of the in-line resonators [9], [10], the proposed CRD allows for independent tuning of the passbands and stopbands and facilitates asymmetrical transfer functions with different BWs.

To further demonstrate the merits of the vertically stacked multiband BPF approach, a triple-band BPF with two

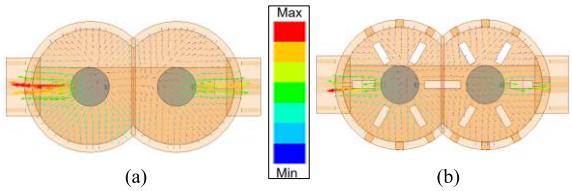

Fig. 5. Surface current distribution at 3.7 GHz of the dual-band vertically integrated BPF. (a) Solid filter walls. (b) With nonradiating slots.

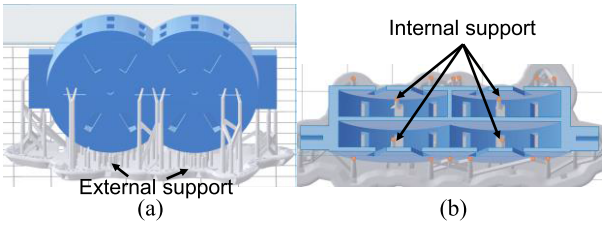

Fig. 6. CAD model of the dual-band BPF for SLA 3-D printing including external and internal support structures. (a) Side view. (b) Cross section showing the internal support structures.

Fig. 7. Manufactured prototypes of the vertically integrated multiband BPFs before and after Cu-plating. (a) Dual-band. (b) Triple-band.

second-order bands was designed. Its three bands are centered at $f_{c1} = 3.6$, $f_{c2} = 4.0$, and $f_{c3} = 4.4$ GHz with $\text{FBW}_1 = 10.3\%$, $\text{FBW}_2 = 6.0\%$, and $\text{FBW}_3 = 7.6\%$, respectively. Its dimensions are listed in Fig. 3 (its EM simulated response is provided in Fig. 8) and correspond to an AR of 2.47. It should be noted that if the same CRD were to be implemented with all of the resonators placed on the same plane, then an AR of 13.2 would be obtained demonstrating a significant 5× AR improvement.

III. Manufacturing and Measurement

For the proof-of-concept validation purposes, the proposed vertically stacked dual-band and triple-band BPFs were manufactured using SLA. To facilitate metallization, nonradiating slots are added on the cavity walls to allow for the Cu chemicals to flow inside the BPF volume. The orientation of the slots must be parallel to the surface currents to prevent radiation, as shown in Fig. 5, for the case of a dual-band BPF with and without the nonradiating slots.

To enable monolithic SLA printing, the filter orientation, the number, and location of the support structures need to be appropriately selected to achieve printability while using a minimal number of internal support structures. As shown in Fig. 6(a), external support structures are placed beneath the filter and can be readily removed after the printing. To avoid deformation of the inner structure, a few internal supports are added to support the post of resonators, as shown in Fig. 6(b). They are mechanically removed after the printing through the nonradiating slots. A commercially available Cu-plating process with a uniform 50-μm copper thickness (>20× skin depth at operating frequency) is applied to all filter parts.

The SLA printed prototype of the dual-band and triple-band BPFs before and after Cu-plating is shown in Fig. 7(a) and (b). The measured S-parameters are shown in Fig. 8(a) and (b), and their respective performance is listed in Table I. In particular, for the dual-band BPF, the effective quality factor (Q_{eff}) is

TABLE I
Comparison With the State-of-the-Art Multiband Coaxial BPFs

Ref	Tech.	f_c (GHz)	FBW (%)	Q_{eff}	AR
[5]	CNC	1.2/5.8	3.7/1.7	1190	3.48
[7]	CNC	0.9/1.8	1.1/0.6	1140	2.47
[8]	CNC	0.9/1.8	30/15	500	3.39
[9]	CNC	0.85/0.9	2.9/1.6	N/A	4.21
[10]	SLA	3.5/3.7/4	4.5/2.7/5.5	1300	17
TW	SLA	3.6/4.2	10.5/7.9	750	3.5
TW	SLA	3.5/4/4.4	13/5.0/5.7	1030	2.37

(TW: this work, AR: axial ratio. Q_{eff}: maximum Q_{eff} of all passbands)

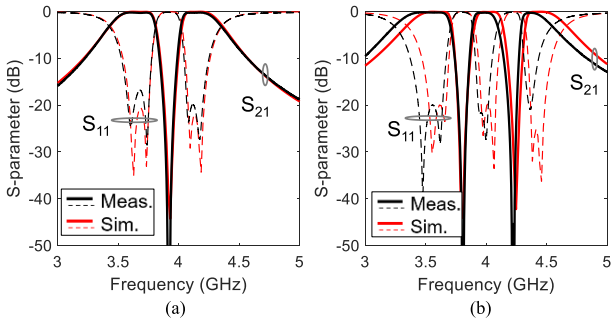

Fig. 8. EM-simulated and RF-measured S-parameters. (a) Dual-band second-order BPF. (b) Triple-band second-order BPF.

670 and 750, while for the triple-band case, $Q_{\text{eff}} = 640$, 1030, and 900. The minor frequency shift for the passbands of the triple-band BPF is due to manufacturing tolerances. Overall, a decent agreement has been achieved between measurements and simulations, successfully validating the vertically integrated multiband coaxial BPF concept.

A comparison with the state-of-the-art multiband coaxial BPFs is provided in Table I. As it can be seen, the proposed multiband BPF is able to realize transfer functions with higher number of passbands (>2), which is otherwise challenging for conventional stepped impedance resonator-based filters, see [5], [6], [7], [8]. Furthermore, the use of monolithic SLA printing has resulted in smaller size and weight and similar Q_{eff} when compared to traditional CNC-machined filters as for example the ones in [5], [7], and [8]. Compared to the work in [10], an 8× AR improvement is achieved for the case of the triple-band BPF. Furthermore, it is based on a distinct CRD, facilitating the realization of asymmetrical passbands. Finally, the proposed concept allows for more complicated multiband configurations to be realized when compared to the single-band BPF in [15].

IV. Conclusion

This letter reported on a new class of compact coaxial cavity resonator-based multiband BPFs. Size compactness is achieved by using vertically stacked coaxial resonators and monolithic 3-D printing. A unique CRD is proposed for multiband BPFs that facilitate independent control of each passband and stopband and asymmetrical responses. A dual-band and a triple-band BPFs were demonstrated for concept validation.

REFERENCES

[1] S.-X. Zhang, L.-L. Qiu, and Q.-X. Chu, "Multiband balanced filters with controllable bandwidths based on slotline coupling feed," *IEEE Microw. Wireless Compon. Lett.*, vol. 27, no. 11, pp. 974–976, Nov. 2017.

[2] K. Zhou, C.-X. Zhou, H.-W. Xie, and W. Wu, "Synthesis design of SIW multiband bandpass filters based on dual-mode resonances and split-type dual- and triple-band responses," *IEEE Trans. Microw. Theory Techn.*, vol. 67, no. 1, pp. 151–161, Jan. 2019.

[3] D. C. H. Bong, V. Jeoti, S. Cheab, and P. W. Wong, "Design and synthesis of chained-response multiband filters," *IEEE Access*, vol. 7, pp. 130922–130936, 2019.

[4] R. R. Mansour, "Filter technologies for wireless base stations," *IEEE Microw. Mag.*, vol. 5, no. 1, pp. 68–74, Mar. 2004.

[5] Z.-C. Zhang, H.-J. Li, X.-Z. Yu, Y. He, and S.-W. Wong, "Dual-narrowband/wideband filters using modified coaxial cavities with large frequency ratios," *IEEE J. Microw.*, vol. 2, no. 4, pp. 690–698, Oct. 2022.

[6] Q.-X. Chu and Z.-C. Zhang, "Dual-band helical filters based on nonuniform pitch helical resonators," *IEEE Trans. Microw. Theory Techn.*, vol. 65, no. 8, pp. 2886–2892, Aug. 2017.

[7] F.-C. Chen, J.-M. Qiu, S.-W. Wong, and Q.-X. Chu, "Dual-band coaxial cavity bandpass filter with helical feeding structure and mixed coupling," *IEEE Microw. Wireless Compon. Lett.*, vol. 25, no. 1, pp. 31–33, Jan. 2015.

[8] Y. Xie, F.-C. Chen, Q.-X. Chu, and Q. Xue, "Dual-band coaxial filter and diplexer using stub-loaded resonators," *IEEE Trans. Microw. Theory Techn.*, vol. 68, no. 7, pp. 2691–2700, Jul. 2020.

[9] G. Macchiarella and S. Tamiazzo, "Design techniques for dual-passband filters," *IEEE Trans. Microw. Theory Techn.*, vol. 53, no. 11, pp. 3265–3271, Nov. 2005.

[10] K. Zhao and D. Psychogiou, "Monolithic multiband coaxial resonator-based bandpass filter using stereolithography apparatus (SLA) manufacturing," *IEEE Trans. Microw. Theory Techn.*, vol. 70, no. 9, pp. 4156–4166, Sep. 2022.

[11] W. J. Otter and S. Lucyszyn, "3-D printing of microwave components for 21st century applications," in *Proc. IEEE MTT-S Int. Microw. Workshop Ser. Adv. Mater. Process. RF THz Appl. (IMWS-AMP)*, Chengdu, China, Jul. 2016, pp. 1–3.

[12] Y. Chen et al., "3-D printed dual-band filter based on spherical dual-mode cavity," *IEEE Microw. Wireless Compon. Lett.*, vol. 31, no. 9, pp. 1047–1050, Sep. 2021.

[13] G. Venanzoni, M. Dionigi, C. Tomassoni, and R. Sorrentino, "3-D-printed quasi-elliptical evanescent mode filter using mixed electromagnetic coupling," *IEEE Microw. Wireless Comp. Lett.*, vol. 28, no. 6, pp. 497–499, Jun. 2018.

[14] E. Lopez-Oliver et al., "3-D-printed compact bandpass filters based on conical posts," *IEEE Trans. Microw. Theory Techn.*, vol. 69, no. 1, pp. 616–628, Jan. 2021.

[15] K. Zhao and D. Psychogiou, "A monolithic vertical integration concept for compact coaxial-resonator-based bandpass filters using additive manufacturing," *IEEE Microw. Wireless Compon. Lett.*, vol. 31, no. 6, pp. 689–692, Jun. 2021.

[16] D. Psychogiou, R. Gomez-Garcia, and D. Peroulis, "Fully adaptive multiband bandstop filtering sections and their application to multifunctional components," *IEEE Trans. Microw. Theory Techn.*, vol. 64, no. 12, pp. 4405–4418, Dec. 2016.